INVESTIGATIONS OF OTR POLARIZATION EFFECTS IN BEAM-PROFILE MONITORS*

A.H. Lumpkin, A.S. Johnson, J. Ruan, and R. Thurman-Keup
Fermilab, Batavia IL, 60510 USA

Abstract

Further investigations of the effects of optical transition radiation (OTR) polarization components on beam profiles are presented. The Fermilab A0 photoinjector is used to generate 14-MeV electron beams which are imaged using OTR. The transverse profiles are examined using the OTR perpendicular and parallel polarization components with respect to the dimension of interest. We observed 10-15% projected profile size reductions on a 65-micron beam size case with the perpendicularly polarized components.

INTRODUCTION

The characterization of transverse beam size using optical transition radiation (OTR) imaging [1-3] is a well-established technique at many accelerators including the Fermilab A0 photoinjector (A0PI) facility. However, there is growing empirical evidence that the utilization of the polarization component orthogonal to the dimension of interest results in a smaller observed projected image profile as theoretically evaluated previously [4-6]. We have continued investigations of this phenomenon with a more controlled experiment where the linear polarizers are selectable in a filter wheel which also included a blank glass position to compensate for the optical path. The aperture for light collection at the polarizer position is thus kept fixed compared to our previous tests [7]. We also have balanced the digital camera gain to present similar signal levels to the data analysis program for both the total OTR and the polarized components. At the relatively low gamma of 30, the horizontal polarization component of OTR is more intense than the vertical one in our optical solid angle. We observed projected profile size reductions on a 65-micron beam size case with the perpendicularly polarized components, and this anomalous effect is compared to results from a standard OTR point-spread-function (PSF) model [4-6].

EXPERIMENTAL ASPECTS

The tests were performed at the Fermilab A0 photoinjector facility which includes an L-band photocathode (PC) rf gun and a 9-cell SCRF accelerating structure which combine to generate up to 16-MeV electron beams. The drive laser operates at 81.25 MHz although the micropulse structure is counted down to 1 MHz. Due to the low electron-beam energies and OTR signals, we typically summed over micropulses depending on the charge per micopulse. Micropulse charges from 25 to 500 pC were used for beam sigma sizes of 45 to 250 microns. The prototype station was installed in the user beam line section beyond the horizontal spectrometer in the straight ahead line as indicated in Fig. 1. The nominal beam parameters are given in Table 1.

The prototype station (see Fig. 2) consists of the vacuum cross with a three-position pneumatic actuator allowing selection of a beam-impedance matching screen, a 100-μm thick YAG:Ce single crystal with its surface normal to the beam direction followed by a 45 degree turning mirror, or a 1-μm thick Al foil for OTR followed by a 45 degree turning mirror. For the OTR polarization tests we removed the thin first foil and used the turning mirror as the OTR screen. We refocused the optics by translating the optical assembly back from the viewing window by 12.5 mm so the center of this OTR screen was in focus. For these tests both turning mirrors were an aluminized Si substrate (200 μm thick). As part of the optics design, a back-illuminated virtual target option with matched field lens could be selected by inserting a beam splitter into the relay optics path. This scene was then relayed to the final Computar zoom lens mounted on the 1.3 Megapixel Prosilica CCD camera and used for resolution and optics calibration aspects. The optical resolution tests were reported previously [8]. A filter wheel was used to select neutral density filters or one of the two linear polarizers which were oriented with the axes in the horizontal and vertical directions. This prototype station was constructed by RadiaBeam Technologies under a contract with Fermilab.

The optical system has 14 (7) μm rms spatial resolution when covering a vertical field of view (FOV) of 18 (5) mm. The calibration factors were 18.2 μm per pixel and 5.4 μm per pixel, respectively. Because of the size of the polarization effects, the data are reported for the higher magnification and 5-mm FOV.

Table 1: Summary of nominal electron beam parameters for operations at 250 pC per micropulse and a drive laser bunch length of 2.7 ps (sigma).

Parameter	Units	Value
Energy	MeV	15
Energy spread	kev	10-15
Transverse Emittance	mm mrad	2.6 ± 0.3
Bunch length	ps	3.1 ± 0.3

*Work supported by Fermi Research Alliance, LLC under Contract No. DE-AC02-07CH11359 with the United States Department of Energy
#lumpkin@fnal.gov

ISBN 978-3-95450-117-5

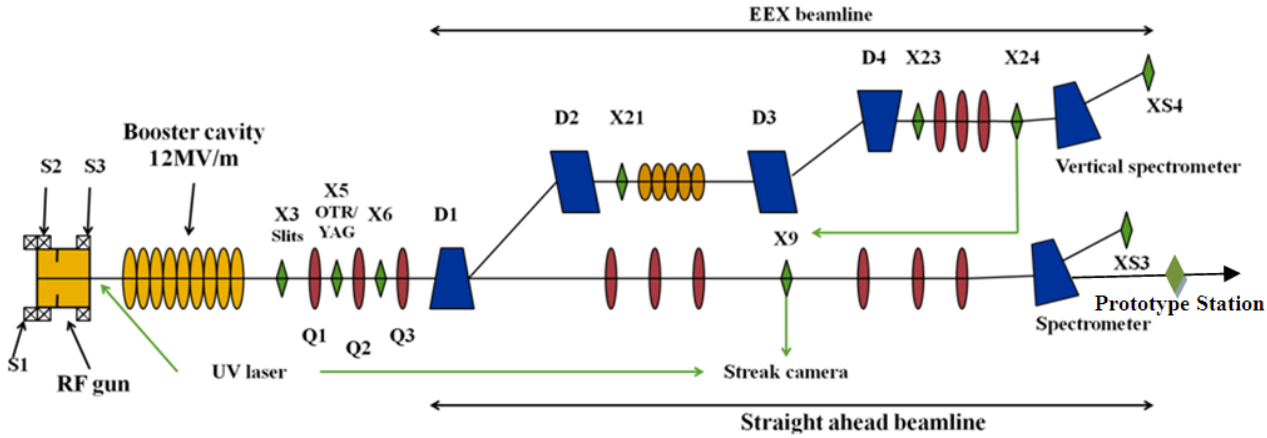

Figure 1: A schematic of the A0 photoinjector test area showing the PC rf gun, 9-cell booster cavity, transverse emittance stations, the OTR stations, the streak camera, and the EEX beamline with the two doglegs, 5-cell deflecting mode cavity, transverse emittance stations, and spectrometer. The prototype station location is indicated.

EXPERIMENTAL RESULTS

The fundamental issue is whether one can detect a measurable difference in beam profile sizes if we use the perpendicular component of OTR, and if so, what is the magnitude? We used focusing by upstream quadrupoles to generate narrow vertical and horizontal stripes at the station. Examples of the images are shown in Fig. 3. The total OTR is at the left and the vertically polarized at the right. The Gaussian fits are used on the projected profiles from the region of interest and are shown below each image. In this case they are 12.6±0.06 and 10.4±0.20 pixels, respectively.

The results are tabulated in Table 2. The camera gain was adjusted to balance the signal levels being processed. Ten image individual averages were done with the Image Tool program and the average variance was divided by $10^{1/2}$. With a calibration factor of 5.3 μm per pixel, we see an ~10-μm reduction (15%) in the initial 65-μm x size when using the perpendicular OTR component.

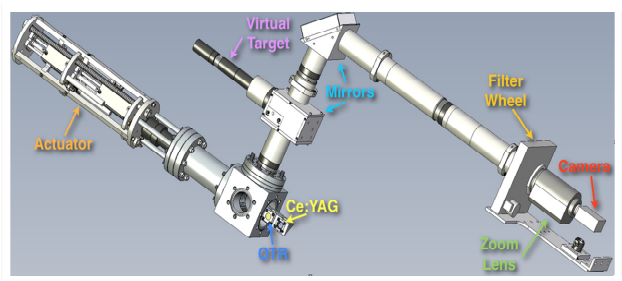

Figure 2: The prototype station with cube and actuator, screens, virtual target, optics, filter wheels, zoom lens, and camera.

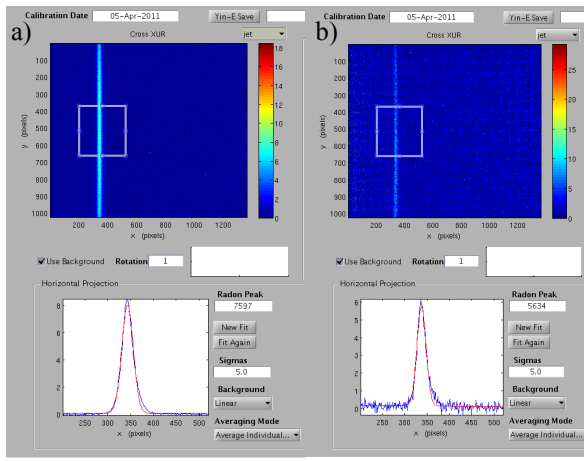

Figure 3: OTR images of vertical stripes a) total OTR and b) vertically polarized OTR. The projected x profiles from the region of interest are shown below each image.

Table 2: Summary of vertical-stripe data. The vertical (V) polarization data are indicated in determining the x sizes. The calibration factor is 5.3 μm per pixel.

Polarization	Amplitude	Position (pixel)	X-sigma (pixel)
No	8.0	343	12.6±0.06
V	5.8	347	10.4±0.20
No	6.4	344	12.7±0.07
No	6.4	344	13.1±0.07
V	3.1	348	11.2±0.10
V	5.1	348	11.4±0.10

ISBN 978-3-95450-117-5

Examples of the horizontal images are shown in Fig. 4. The total OTR is at the bottom and the horizontally polarized OTR image at the top. The Gaussian fits are used on the projected y profiles from the region of interest and are shown beside each image. In this case they are 11.8±0.11 and 10.5±0.12 pixels, respectively.

The results are tabulated in Table 3. The camera gain was adjusted to balance the signal levels being processed. Ten image individual averages were done with the Image Tool program and the average variance was divided by $10^{1/2}$. With a calibration factor of 5.3 um per pixel, we see an ~6-μm reduction (10%) in the initial 62-μm y size with the perpendicular OTR component. We note that at this low gamma of 30 with rotation around a vertical axis, the horizontal polarized `angular pattern is asymmetric in lobe intensity and shape while the vertical component lobes are symmetric. The broken symmetry in one plane is not in the model described in the next section.

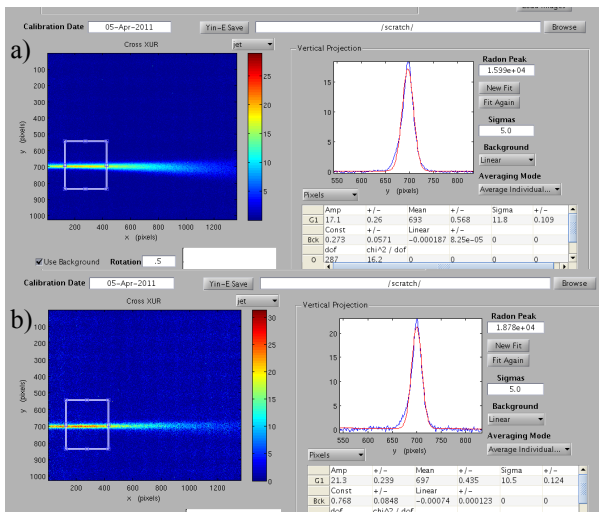

Figure 4: OTR images of horizontal stripes a) total OTR and b) vertically polarized OTR. The projected y profiles from the region of interest are shown beside each image.

Table 3: Summary of horizontal-stripe data. The horizontal (H) polarization data are indicated in determining the y sizes.

Polarization	Amplitude	Position (pixel)	Y-sigma (pixel)
No	17	692	11.8±0.11
H	21	697	10.5±0.10
No	(17)	692	11.5±0.10
H	20	694	10.5±0.10
H	21	691	10.2±0.09
No	17	691	11.6±0.12

OTR POINT-SPREAD-FUNCTION MODEL

The assessment of the actual OTR point spread function has to first order been described by several authors previously [5,6]. The model invokes the convolution of the basic OTR single particle angular distribution function with the J_1 ordinary Bessel function to describe the intensity pattern at the detector. The idea is to calculate the electric field distribution at the image plane and then square it to get the photon intensity distribution I(x,y) expected. This is described in ref. [5,6] and shown in the expression below for a single ideal lens:

$$I(x,y) \propto \left[\int \frac{\theta^2}{\theta^2 + 1/\gamma^2} \cdot J_1\left(\frac{k\theta\sqrt{x^2+y^2}}{M} \right) d\theta \right]^2 ,$$

where $k = 2\pi/\lambda$ with λ the wavelength of radiation , x and y are the spatial coordinates, magnification=M, the angle of OTR emission is θ, and the Lorentz factor is γ. The angle of integration is limited by the aperture of the lens (θ_{max}), and this can have a strong effect on the PSF in the model.

Because at the simplest level OTR has an annular angular distribution, the point spread function does reflect this aspect in the upper left image of Fig. 5. Note the axes scales are ±100 μm. The horizontal polarization component appears as a double lobe as seen in Fig. 5b, while the vertical polarization is seen also as a double lobe in Fig. 5c. These are *not* far-field angular distribution patterns, but the PSF in the image plane. The projections of these are shown overlaid in Fig. 6 where the total (blue curve), horizontal polarization with horizontal projection (red curve), and horizontal polarization with vertical projection (green curve) exhibit different features.

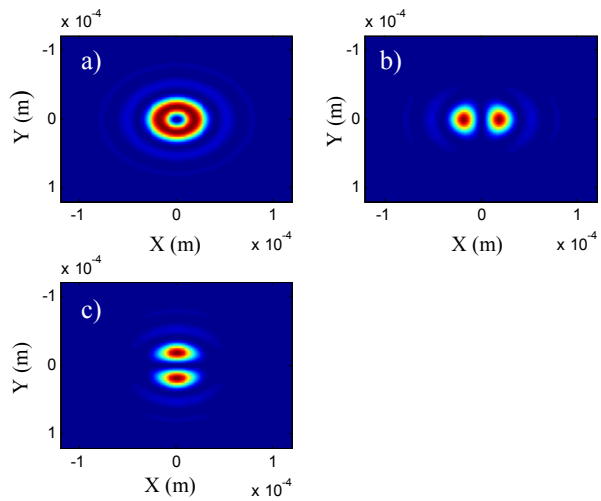

Figure 5: OTR PSF images with a) total, b) horizontal polarization, and c) the vertical polarization of the case: Energy=14.3 MeV, M=1, λ=500 nm, θ_{max}=0.010, and σ=25μm.

ISBN 978-3-95450-117-5

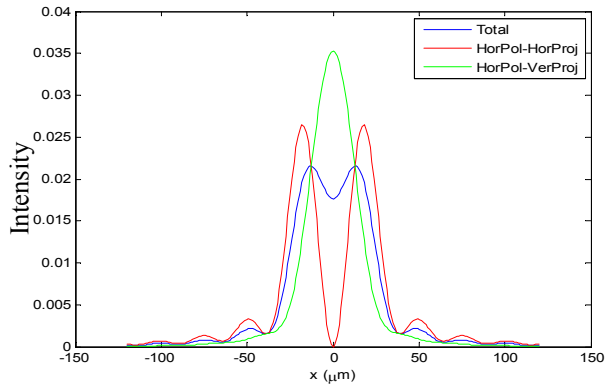

Figure 6: OTR PSF projections of the images in Fig. 5 with total, horizontal polarization with horizontal projection, and the vertical projection of the same case.

We next show in Fig. 7 the results of convolving the initial beam size of σ=25 μm with the OTR PSF projections of Fig. 6: The results of the Gaussian fits to the convolved profiles are: Total 33.1 μm, horizontal polarization 38.0 μm, and the vertical projection of the horizontal polarization 29.3 μm. The model does support the concept that use of the perpendicularly polarized component is closer to the original 25 μm size than using the Total or parallel components. Even in this vertical projection case one would still need to deconvolve the PSF to get the actual beam size. This several-micron effect was generated by using the 10-mrad acceptance angle, which is smaller than one might expect for our optics and a two times smaller beam size. The results for convolving an initial 50-μm beam size and the OTR PSF are: total 55.6 μm, horizontal polarization 58.5 μm , and vertical projection 53.0 μm. The effects are relatively smaller and symmetrically change around the total value.

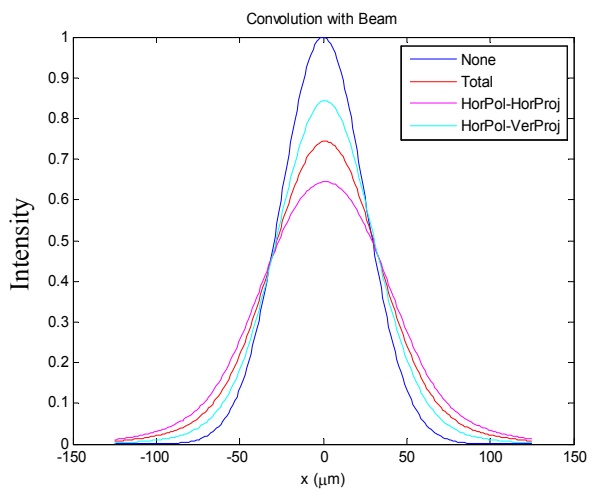

Figure 7: Comparison plots of the original x size (25 μm) with no convolution and convolutions with the OTR PSF projections of the total (33.1 μm), horizontal polarization-horizontal projection (38.0 μm), and the vertical projection (29.3 μm) of the same latter case.

The experimental data in the tables suggest an asymmetry that is not in this simplified model. A more extreme case is described in ref. 9 where the beam size in the vertical plane is only 2.2 μm, and the PSF's double lobe for their optical system is actually visualized in the image.

SUMMARY

We have detected an apparent polarization-dependent beam profile size for OTR images. In this case and configuration we see projected profile reductions of 15% in x and 10% in y relative to the total radiation image profile. The magnitude of the experimental effect is only approached in the model by reducing the solid angle subtended by the optics and halving the beam size. The observed asymmetry of the effect is not addressed in the model. We still find that the OTR polarization effects are analogous to what was observed in optical diffraction radiation experiments in the past [10] which may be attributed to the time-averaged induced-current distribution in the metal surface.

ACKNOWLEDGMENTS

The authors acknowledge J. Santucci for beamline integration issues and the support of M. Wendt, N. Eddy, E. Harms, and M. Church of the Fermilab Accelerator Division.

REFERENCES

[1] L. Wartski et al., Journ. Appl. Phys., **46**, 3644 (1975).
[2] R.B. Fiorito and D.W. Rule, p.21, Conf. Proc. No.319, BIW94, Robert E. Shafer, ed. AIP (1994).
[3] A. H. Lumpkin et al., "Initial Imaging of 7-GeV Electron Beams with OTR/ODR Techniques at the APS", Proc. of PAC05, Knoxville, Tenn., p.4162. (2005), http://www.JACoW.org.
[4] V.A. Lebedev, Nucl. Instr. in Phys. Res. **A372**, 344 (1996).
[5] M. Castellano and V.A.Verzilov, Phys. Rev. ST Accel. Beams, 1:062801 (1998).
[6] Rasmus Ischebeck et al., Proc. of PAC05, Knoxville, Tenn., p. 4042, http://www.JACoW.org.
[7] A.H. Lumpkin et al., "OTR Polarization effects in Beam profile Monitors at the Fermilab A0 Photo-injector", Proc. of BIW10, May 2010, Santa Fe, NM, TUPSM001, http://www.JACoW.org.
[8] A.H. Lumpkin et al., "Initial Beam-Profiling Tests with the NML Prototype Station at the Fermilab A0 Photoinjector" , Proc. of PAC11, New York, NY, MOP219, (2011), http://www.JACoW.org.
[9] A. Aryshev et al., Proc. of IPAC10, Kyoto, Japan, MOPEA052, 195 (2010), http://www.JACoW.org.
[10] Pavel Evtushenko et al., "Near-Field ODR Measurements at CEBAF" , Proc. of BIW08, Lake Tahoe, CA, p.332, (2008), http://www.JACoW.org.

ISBN 978-3-95450-117-5